Crystals **2014**, *4*, 209-227; doi:10.3390/cryst4030209

OPEN ACCESS

crystals

ISSN 2073-4352

www.mdpi.com/journal/crystals

Article

Combinatorial Frequency Generation in Quasi-Periodic Stacks of Nonlinear Dielectric Layers

Oksana Shramkova and Alexander Schuchinsky *

School of Electronics, Electrical Engineering & Computer Science, Queen's University Belfast, Queen's Road, Queen's Island, Belfast BT3 9DT, UK; E-Mail: o.shramkova@qub.ac.uk

***** Author to whom correspondence should be addressed; E-Mail: a.schuchinsky@qub.ac.uk; Tel.: +44-28-9097-1736; Fax: +44-28-9097-1702.

Received: 10 May 2014; in revised form: 6 June 2014 / Accepted: 9 June 2014 / Published: 1 July 2014

Abstract: Three-wave mixing in quasi-periodic structures (QPSs) composed of nonlinear anisotropic dielectric layers, stacked in Fibonacci and Thue-Morse sequences, has been explored at illumination by a pair of pump waves with dissimilar frequencies and incidence angles. A new formulation of the nonlinear scattering problem has enabled the QPS analysis as a perturbed periodic structure with defects. The obtained solutions have revealed the effects of stack composition and constituent layer parameters, including losses, on the properties of combinatorial frequency generation (CFG). The CFG features illustrated by the simulation results are discussed. It is demonstrated that quasi-periodic stacks can achieve a higher efficiency of CFG than regular periodic multilayers.

Keywords: quasi-periodic structure; nonlinear dielectric; nonlinear scattering; three-wave mixing; combinatorial frequency generation; Fibonacci stack; Thue-Morse sequence

---

1. Introduction

The recent theoretical and experimental studies of nonlinear metamaterials (MM) and photonic crystals (PhC) have demonstrated potential of their applications in functional devices operating in diverse frequency ranges, from microwaves to optics. Traditionally, artificial media have periodic order with regular spectral characteristics. In contrast, long-range order of quasi-periodic structures (QPSs) and quasi-crystals provides additional degrees of freedom and enables new unusual properties, which recently attracted considerable interest [1].

QPSs with high order symmetry lie between periodic crystals and random amorphous solids. Since the first realization of Fibonacci and Thue-Morse type superlattices [2], the physical properties of 1-D QPSs have been extensively studied, both experimentally and theoretically, and it has been shown that QPSs can exhibit unique features unattainable in periodic arrangements. In particular, it was found that QPSs create localization of electronic states and their collective response differs from that of their constituents. While the linear wave phenomena in quasi-periodic media were extensively explored during the last few decades [3–24], nonlinear QPSs have been studied only recently [25–35].

The main distinctive features of nonlinear artificial media are usually associated with their ability to simultaneously control the dispersion and nonlinear interactions by altering both the geometry of constituent particles and their arrangements in ensembles. Both periodic and quasi-periodic nonlinear structures have been studied primarily with the aim of improving harmonic generation efficiency. QPSs with additional degrees of freedom due to the higher order group symmetry are particularly attractive for creating higher density of states that can facilitate harmonic generation [36–38]. It has been observed in [25] that the efficiency of second-harmonic generation (SHG) in QPS is higher than in random medium, but still remains lower than in regular periodic structures. On the other hand, an eight-fold increase of the third-harmonic generation (THG) efficiency has been attained in the two-step cascaded process in a QPS as compared with a similar periodic multilayer [26].

Combinatorial frequency generation (CFG) by mixing pump waves of different tones enables more versatile spectrum control. However, the dominant three- and four-wave mixing processes are usually demanding to not only the nonlinearity itself but also the linear dispersion and field distribution, which primarily depend on the medium intrinsic properties and composition. Therefore, QPSs with their rich spectral properties may provide favourable conditions for frequency mixing and CFG. To realise this potential, it is important to explore in detail the mechanisms and features of CFG in QPSs.

In this paper, a generic approach to the analysis of CFG by layered QPSs, illuminated by two obliquely incident pump waves, has been developed and applied to the study of the properties of frequency mixing products. The problem statement and solution of the boundary value problem for the Fibonacci and Thue-Morse type QPSs are outlined in Section 2 and elaborated in Appendices. The features of CFG by the QPSs composed of nonlinear anisotropic dielectric multilayers are illustrated by the results of numerical simulations and discussed in Section 3. The main findings are summarised in Conclusion.

2. Problem Statement and Methodology

QPSs shown in Figure 1 are composed of stacked weakly nonlinear anisotropic dielectric layers of two kinds (labelled *A* and *B*) with thicknesses d_A and d_B, respectively. Stacks of thicknesses L_q are surrounded by a linear homogeneous medium with the relative permittivity ε_a at $z \leq 0$ and $z \geq L_q$. The constituent dielectric layers with quadratic nonlinearity and 6 mm class of anisotropy are described by the tensors of relative linear permittivity $\hat{\varepsilon}_j = (\varepsilon_{xx}, \varepsilon_{xx}, \varepsilon_{zz})_j$ and nonlinear susceptibility $\hat{\chi}_j$ where $j = A, B$:

$$\hat{\chi}_j = \begin{pmatrix} 0 & 0 & 0 & 0 & \chi_{xxz} & 0 \\ 0 & 0 & 0 & \chi_{xxz} & 0 & 0 \\ \chi_{zxx} & \chi_{zxx} & \chi_{zzz} & 0 & 0 & 0 \end{pmatrix}_j \quad (1)$$

The stacked layers are arranged in accordance with the following quasi-periodic sequences:

(a) Fibonacci type QPS (Figure 1a) of order $q \geq 2$ is defined recursively by the recurrence relation: $S_q = \{S_{q-1} \cup S_{q-2}\}$, where $S_0 = \{B\}$, $S_1 = \{A\}$; the number of layers in a stack S_q equals Fibonacci number Φ_{q+1} and the corresponding stack thickness is $L_q = L_{q-1} + L_{q-2}$ with $L_0 = d_B$, $L_1 = d_A$;

(b) Thue-Morse type QPS (Figure 1b) of order $q \geq 1$ is defined recursively by the recurrence relations: $Q_q = \{Q_{q-1} \cup Q'_{q-1}\}$ and $Q'_q = \{Q'_{q-1} \cup Q_{q-1}\}$, where Q_q and Q'_q are complementary to each other and $Q_0 = \{A\}$, $Q'_0 = \{B\}$; the stacks Q_q and Q'_q contain 2^q layers and have thicknesses $L_q = L'_q = (d_A + d_B)^q$ at $q > 0$ and $L_0 = d_A$, $L'_0 = d_B$.

Figure 1. Geometry of the problem: (**a**) Fibonacci type QPS; (**b**) Thue-Morse type QPS.

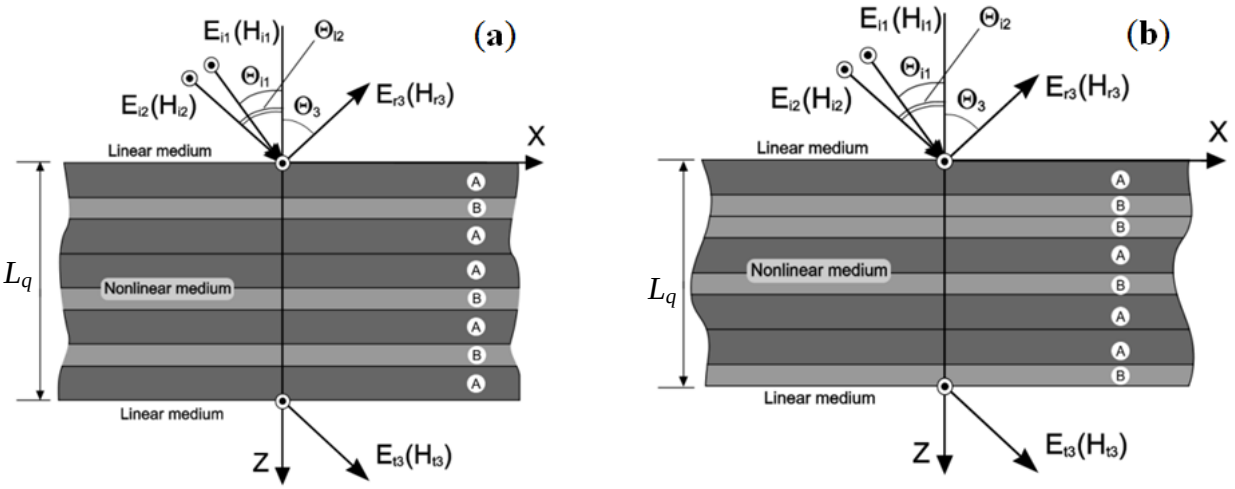

The stacks are illuminated by two pump plane waves of frequencies ω_1 and ω_2 incident at angles Θ_{i1} and Θ_{i2}, respectively. Since the layers are assumed isotropic in the *x*-*y* plane, the TE and TM polarised waves with the fields independent of the *y*-coordinate $(\partial/\partial y = 0)$ can be analysed separately. Only TM waves with the field components E_x, E_z, H_y are presented in the paper. The TE waves are treated similarly and even somewhat simpler, because the nonlinear susceptibility given by Equation (1) is isotropic for TE polarised waves.

To evaluate the characteristics of TM waves of combinatorial frequencies generated by a nonlinear QPS, the fields of both pump waves and their mixing products inside the stack are to be determined first. Assuming that nonlinearity of the constituent layers is weak and the three-wave mixing process is dominant, the nonlinear products can be obtained by the harmonic balance method. At combinatorial frequency $\omega_3 = \omega_1 + \omega_2$ the TM wave fields in each layer are described by non-homogeneous Helmholtz equation:

$$\frac{\partial^2 H_{yj}(\omega_3)}{\varepsilon_{xxj}\partial z^2}+\left(k_3^2-\frac{k_{x3}^2}{\varepsilon_{zzj}}\right)H_{yj}(\omega_3)=4\pi k_3\left[2\frac{\partial}{\partial x}\left(\frac{\chi_{zxxj}}{\varepsilon_{zzj}}E_{xj}(\omega_1)E_{xj}(\omega_2)+\frac{\chi_{zzzj}}{\varepsilon_{zzj}}E_{zj}(\omega_1)E_{zj}(\omega_2)\right)-\right.$$
$$\left.\frac{\chi_{xxzj}}{\varepsilon_{xxj}}\frac{\partial}{\partial z}\left(E_{xj}(\omega_1)E_{zj}(\omega_2)+E_{xj}(\omega_2)E_{zj}(\omega_1)\right)\right] \quad (2)$$

where $E_{xj}(\omega_{1,2})$ and $E_{zj}(\omega_{1,2})$ are the electric field components of pump waves in a layer of type $j = A, B$; $k_3=\omega_3/c$ and $k_{x3}=k_3\sqrt{\varepsilon_a}\sin\Theta_3$; angle Θ_3 defines the emission direction from the stacks at frequency ω_3, which is determined by the phase synchronism condition in the three-wave mixing process [39]:

$$k_{x3}=k_{x1}+k_{x2} \quad (3)$$

where $k_{x1,x2}=k_{1,2}\sqrt{\varepsilon_a}\sin\Theta_{i1,i2}$, $k_{1,2}=\omega_{1,2}/c$.

The solution of Equation (2) for $H_{yj}(\omega_3)$ can be represented as a superposition of six plane waves with longitudinal propagation constants $\pm k_{zj}^{\pm}$ and $\pm k_{zj}^{(3)}$

$$H_{yj}^{(n)}(\omega_3,x,z)=\left(\mathcal{B}_j^{n+}(\omega_3)e^{ik_{zj}^{(3)}z}+\mathcal{B}_j^{n-}(\omega_3)e^{-ik_{zj}^{(3)}z}+D_{1j}^{n+}e^{ik_{zj}^{+}z}+D_{2j}^{n+}e^{-ik_{zj}^{+}z}+D_{1j}^{n-}e^{ik_{zj}^{-}z}+D_{2j}^{n-}e^{-ik_{zj}^{-}z}\right)e^{-i\omega_3 t+ik_{x3}x} \quad (4)$$

where $k_{zj}^{\pm}=k_{zj}^{(1)}\pm k_{zj}^{(2)}$, $k_{zj}^{(p)}=\sqrt{\varepsilon_{xxj}\left(k_p^2-k_{xp}^2/\varepsilon_{zzj}\right)}$, $p=1,2,3$ and superscript n is a serial number of a primitive cell, which identifies the position of a jth type layer in the stack. $D_{1j,2j}^{n\pm}$ are amplitudes of the waves of frequency ω_3, generated inside this layer, which depend on amplitudes $\mathcal{B}_j^{n\pm}(\omega_{1,2})$ of the pump waves refracted into this layer [40]. $\mathcal{B}_j^{n\pm}(\omega_3)$ are amplitudes of the waves of frequency ω_3 generated outside the layer and refracted into it.

To calculate the amplitude coefficients in Equation (4), it is necessary first to find the pump wave amplitudes in each constituent layer. In periodic stacks comprised of alternating binary layers this is accomplished by the transfer matrix method (TMM) [41–44] as the unit cell layout and serial number n fully identify the layer type (A or B) and position in the stack. This approach can be extended to QPS because the stack composition is defined by the deterministic rules. However, evaluation of each layer position and type in a specific sequence is usually a challenging task.

Examination of Fibonacci and Thue-Morse QPSs shows that they contain only two types of primitive cells. Indeed, Fibonacci QPS, for example, S_6 = {*AB AAB AB AAB AAB*} is comprised of "regular" cells {*AB*} and "defective" cells {*AAB*} with an additional *A* layer which forms a layer *A* doublet of thickness $d'_A = 2d_A$. Similarly, Thue-Morse QPS, for example, Q_4 = {*AB BA BA AB BA AB AB BA*} is composed of the same "regular" cells {*AB*} and "defective" cells {*BA*} with inverse order of layers but the same cell thickness. Thus once the cell serial number n, and layout and position of the regular and defective cells are known, the conventional TMM can be adapted to obtain amplitude coefficients $D_{1j,2j}^{n\pm}$ and $\mathcal{B}_j^{n\pm}(\omega)$ in Equation (4) for Fibonacci and Thue-Morse QPSs as detailed in Appendix 1.

Once the fields of combinatorial frequencies ω_3 in individual layers are determined, amplitudes $F_r(\omega_3)$ and $F_t(\omega_3)$ of the field emitted from stacks toward the reverse and forward directions of the z-axis, respectively, can be evaluated by the modified TMM [40] as described in Appendix 2. The obtained analytical solutions provide an insight in the fundamental mechanisms of nonlinear scattering

and frequency mixing by the QPSs illuminated by a pair of obliquely incident plane waves. The features of CFG in Fibonacci and Thue-Morse QPSs are further illustrated by examples of numerical simulations and discussed in the next section.

3. Simulation Results and Discussion

To elucidate the CFG mechanisms in QPSs, the nonlinear scattering characteristics of TM waves by the stacks of Fibonacci and Thue-Morse sequenced binary anisotropic layers have been analysed numerically. Illustrative examples of the simulation results for the specific QPS arrangements are discussed below in comparison with the corresponding periodic stacks of the same thicknesses.

It is assumed that the stacks are surrounded by air with the relative permittivity $\varepsilon_a = 1$ and are illuminated by a pair of pump plane waves of frequencies $\omega_{1,2}$ incident at angles $\Theta_{i1,i2}$ as shown in Figure 1. The QPS constituent layers are anisotropic dielectric films of CdS and ZnO with the following values of the tensor relative linear permittivity $\hat{\varepsilon}_{A,B}$ and nonlinear susceptibility $\hat{\chi}_{A,B}$ (the $\hat{\chi}_{A,B}$ units [m/V] are omitted below for brevity) [45]:

Layer *A* (CdS): $\varepsilon_{xxA} = 5.382$, $\varepsilon_{zzA} = 5.457$, $\chi_{xxzA} = 2.1 \times 10^{-7}$, $\chi_{zxxA} = 1.92 \times 10^{-7}$, $\chi_{zzzA} = 3.78 \times 10^{-7}$,
Layer *B* (ZnO) $\varepsilon_{xxB} = 1.4$, $\varepsilon_{zzB} = 2.6$, $\chi_{xxzB} = 2.82 \times 10^{-8}$, $\chi_{zxxB} = 2.58 \times 10^{-8}$, $\chi_{zzzB} = 8.58 \times 10^{-8}$.

The layer thicknesses d_A and d_B are related by the golden ratio: $\tau = d_A/d_B = \left(1+\sqrt{5}\right)\Big/2$.

3.1. Spectral Efficiency of Frequency Mixing

The earlier studies of photonic crystals and periodic stacks of dielectric layers have suggested that the SHG and THG efficiency may be higher at the bandgap edges. However, the concurrent increase of losses considerably reduces the gain. Alternatively, CFG efficiency proved to be higher not at the band edges but in the transparency bands, especially at Wolf-Bragg resonances of the stacks [40]. Additionally, CFG involving two pump waves of different frequencies ω_1 and ω_2, incident at dissimilar angles, offers extra degrees of freedom in controlling the frequency mixing process and spectrum.

The frequency mixing efficiency in the stacks of nonlinear layers essentially depends on the phase coherence, which is controlled by linear dispersion of both pump waves and their nonlinear products. Additionally, magnitudes of interacting pump waves are significantly influenced by the stack composition and linear reflectance $R(\omega)$, variable with the incidence angle. Therefore rich spectral content of QPS has potential for assisting CFG enhancement.

To illustrate the effect of the stack composition, $|R(\omega)|^2$ of TM waves incident at angles $\Theta_i = 30°$ and $\Theta_i = 45°$ are displayed in Figure 2 for Fibonacci S_8 (34 layers, $d_B = 12$ μm) and Thue-Morse Q_5 (32 layers, $d_B = 13$ μm) QPSs in comparison with the periodic stack of alternating layers (16 unit cells or 32 layers, $d_B = 13$ μm). All three stacks have the same thickness, and equal number of *A*- and *B*-type layers in the periodic and Thue-Morse stacks, while the Fibonacci QPS contains more layers of smaller thicknesses. Considerable differences in $|R(\omega)|$ of the periodic stack and QPSs are evident in Figure 2, especially at higher frequencies. This implies that the frequency mixing efficiency may significantly vary due to disparity of the pump wave magnitudes refracted into the stack. Bandgaps, corresponding

to $|R(\omega)| \approx 1$, exist in both periodic structures and QPSs, albeit more intricate spectra of QPSs provide more flexible conditions for CFG as discussed below.

Figure 2. Reflectance of TM wave incident at $\Theta_i = 30\,°$ (dashed black lines) and $\Theta_i = 45\,°$ (solid red lines) on (**a**) Fibonacci S_8 and (**b**) Thue-Morse Q_5 QPSs, and (**c**) periodic stack with 16 unit cells.

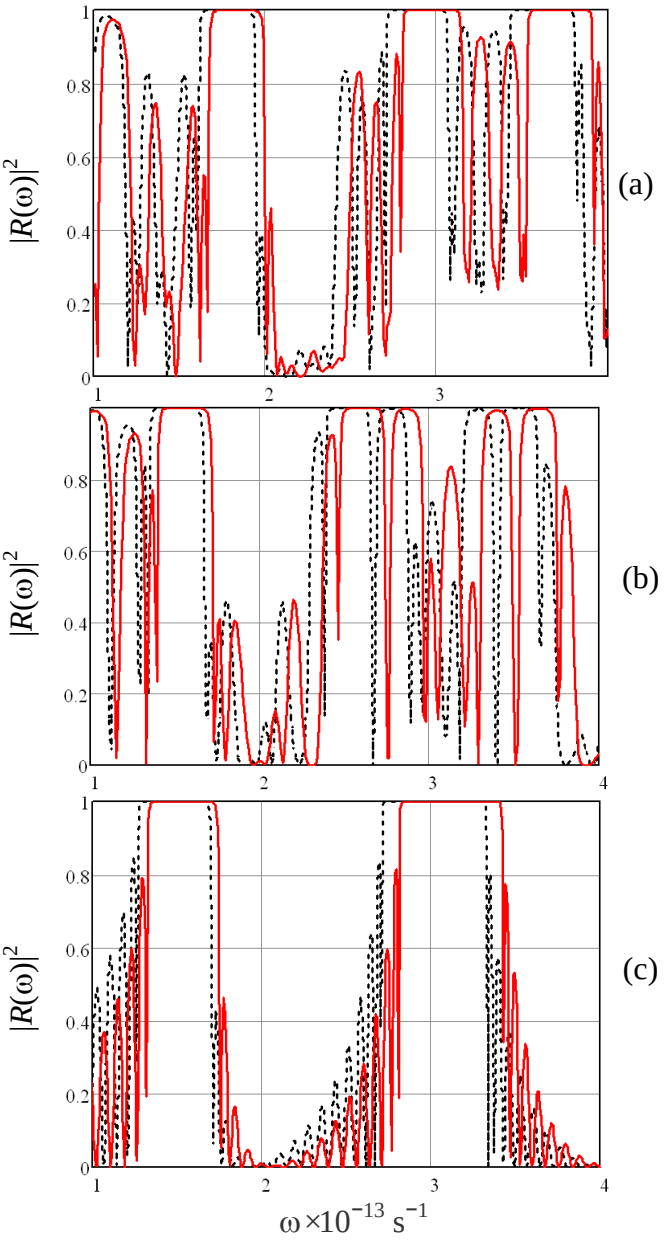

To assess the effect of the pump wave reflectance on CFG, magnitudes $|F_{r,t}(\omega_3)|$ of the waves of combinatorial frequency ω_3 emitted from the stacks have been simulated at fixed frequencies ω_2 of a pump wave incident at $\Theta_{i2} = 45\,°$, and swept frequency ω_1 of the other pump wave incident at $\Theta_{i1} = 30\,°$. Frequencies ω_2 have been chosen individually for each stack configuration so that $|R(\omega_2)|^2$ be at the minima close to the transparency band edges. Since QPS bands are not clearly defined as in periodic stacks, we refer only to the reflectance minima, which depend on the constituent layer parameters and incidence angles of pump waves as illustrated by Figure 2.

Inspection of Figures 2 and 3 demonstrates definite correlation between $|F_{r,t}|$ and $|R(\omega)|$ for each type of QPSs. Indeed, $|F_{r,t}|$ reach their peaks at frequencies ω_1 corresponding to the minima of the pump wave reflectivity, thus confirming that the pump wave refraction into stacks significantly influences the frequency mixing efficiency. It is also evident here that the CFG efficiency is hardly improved in the proximities of band edges for both QPSs and periodic stacks.

Figure 3. Intensity of field radiated from QPSs at frequency $\omega_3 = \omega_1 + \omega_2$ in the reverse ($|F_r|$-solid red lines) and forward ($|F_t|$-dash-dot black lines) directions of the *z*-axis: (**a**) Fibonacci S_8 stack at $\omega_2 = 2.01 \times 10^{13}$ s^{-1}; (**b**) Thue-Morse Q_5 stack at $\omega_2 = 1.73 \times 10^{13}$ s^{-1} and (**c**) periodic stack containing 16 unit cells at $\omega_2 = 1.76 \times 10^{13}$ s^{-1}. All the stacks are illuminated by pump waves incident at $\Theta_{i1} = 30°$ and $\Theta_{i2} = 45°$.

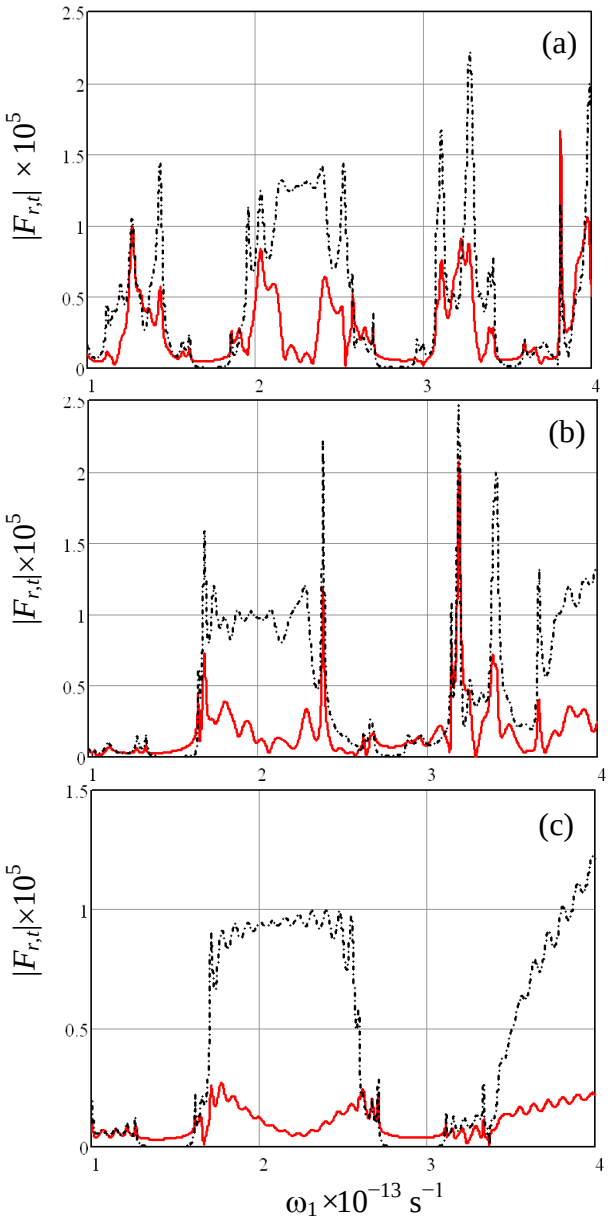

Comparison of $|F_{r,t}|$ for the stacks of the three types shows that the peak CFG efficiency is higher in the QPSs than in the periodic structure. For example, the $|F_r|$ peak at $\omega_1 = 2.38 \times 10^{13}$ s^{-1} in Thue-Morse QPS Q_5 (Figure 3b) is about 2.2 times higher than in the periodic stack (Figure 3c). Such

enhanced CFG is attributed to more favourable conditions for the phase synchronism in the QPS and *local* field intensification in individual constituent layers due to the stack composition. Additionally, the internal refraction of pump waves and concurrent constructive interference of the generated combinatorial frequencies ω_3 in the entire stack lead to cumulative growth of the peak emission in the forward direction (note that almost all peaks of $|F_t|$ in Figure 3 are higher than $|F_r|$ peaks). Examination of the $|F_{r,t}|$ angular dependences has also proven that $|F_{r,t}|$ reach their maxima at the reflectance $|R(\omega)|$ minima of not only pump waves but also the waves of combinatorial frequency ω_3. This implies that the CFG efficiency can be further increased by optimising combinations of the incidence angles, layer parameters, and the stack composition.

3.2. Effect of Stack Composition and Layer Anisotropy

Both the analytical estimations and numerical results shown in Figures 2 and 3 have demonstrated strong effect of the stack internal arrangements on both the reflectance and CFG. To illustrate it further, Figure 4 displays $|F_{r,t}|$ simulated for Fibonacci S_7 stack, containing 21 layer with d_B = 19 μm, and Thue-Morse Q_4 stack, containing 16 layers with d_B = 26 μm, which have the same overall thicknesses as Fibonacci S_8 and Thue-Morse Q_5 QPSs in Figure 3 but thicker constituent layers. Comparison of Figures 3 and 4 shows that intensities $|F_{r,t}|$ of the combinatorial frequency ω_3 emitted from the stacks have almost the same peak magnitudes in both cases but the peaks occur at different frequencies ω_1. Such spectral deviations can be attributed to pump wave redistribution in the stack constituent layers, caused by the internal reflection and refraction at the layer interfaces, and to the changes in the phase coherence between the pump waves and combinatorial frequency waves generated in individual constituent layers.

Figure 4. Intensity of field radiated from QPSs at frequency $\omega_3 = \omega_1 + \omega_2$ in the reverse ($|F_r|$-solid red lines) and forward ($|F_t|$-dash-dot black lines) directions of the *z*-axis: (**a**) Fibonacci S_7 stack at $\omega_2 = 2.02 \times 10^{13}$ s^{-1}; (**b**) Thue-Morse Q_4 stack at $\omega_2 = 1.76 \times 10^{13}$ s^{-1}. All the stacks are illuminated by pump waves incident at $\Theta_{i1} = 30°$ and $\Theta_{i2} = 45°$.

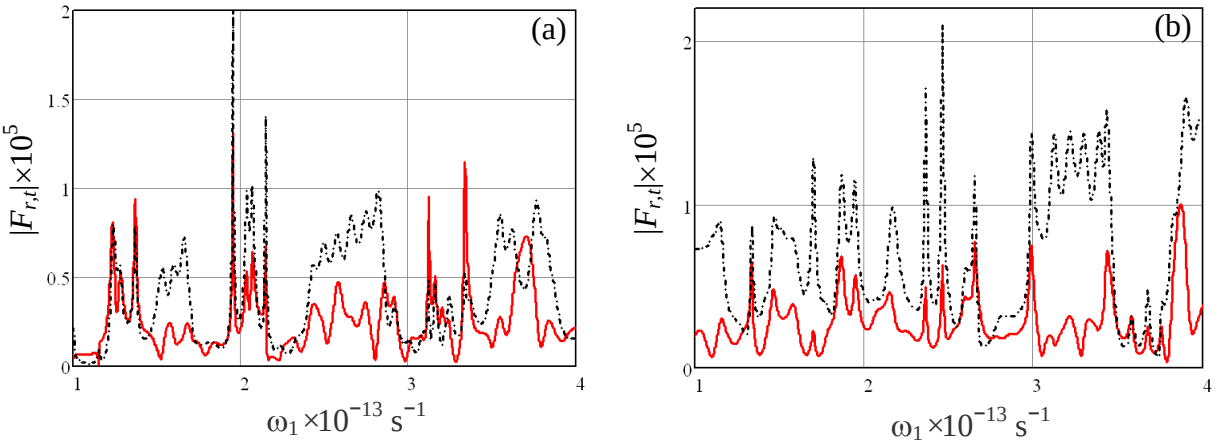

In order to assess the effect of the dielectric layers' anisotropy on CFG, Fibonacci and Thue-Morse QPSs of several different orders q have been re-simulated with isotropic constituent layers. The scalar relative permittivities $\varepsilon_{A,B}$ and nonlinear susceptibilities $\chi_{A,B}$ have been set equal to the tensor components specified above: $\varepsilon_{xxA} = \varepsilon_{zzA} = 5.382$, $\chi_{xxzA} = \chi_{zxxA} = \chi_{zzzA} = 2.1 \times 10^{-7}$ m/V, $\varepsilon_{xxB} = \varepsilon_{zzB} = 1.4$, $\chi_{xxzB} = \chi_{zxxB} = \chi_{zzzB} = 2.82 \times 10^{-8}$ m/V. Comparison of the simulation results for the isotropic and anisotropic layers has shown that the peak intensities of CFG are generally higher in isotropic cases, especially in QPSs with lower order q. The effect of the layer anisotropy in Fibonacci and Thue-Morse stacks appeared to be different. For example, in Fibonacci S_7 stack with isotropic layers $|F_{r,t}|$ peaks are nearly twice as high as in the same stacks with anisotropic layers, whereas in a similar Thue-Morse Q_4 configuration, magnitudes of $|F_{r,t}|$ peaks have about the same magnitudes. These observations suggest that a combination of the stack composition and the constituent layer anisotropy may noticeably influence CFG, especially in QPSs of low orders q. When q increases at fixed stack thickness, the $|F_{r,t}|$ peak magnitudes become closer in the stacks with isotropic and anisotropic layers. The latter trend can be attributed to thinning of the constituent layers that leads to the dominant effect of the spatial anisotropy enhanced by finer stratification of the stacks.

3.3. Effect of Loss

To assess the effect of dissipation on CFG in QPSs, Fibonacci S_8 and Thue-Morse Q_5 stacks with the same layer parameters as in Figure 3 have been simulated taking into account the loss tangents of the constituent layers: $\tan\delta_{xx,zz} = 0.01, 0.1$. Comparison of the simulation results in Figures 3 and 5 (lossless case) shows that the dielectric losses suppress sharp spikes of $|F_{r,t}|$ observed in the lossless QPSs and stronger affect emission in the forward direction than in the reverse direction of the z-axis [46].

The latter effect is particularly evident in Figure 5b,d where $|F_t|$ becomes nearly two orders of magnitude smaller than $|F_r|$. It is also important to note that not only magnitudes but also spectral content of the combinatorial frequencies emitted from the QPSs with imperfect layers qualitatively changes at higher losses.

These results demonstrate that CFG levels in the lossy QPSs are substantially decreased by dissipation of both pump waves and frequency mixing products. Their decays have different spatial scales, and dissimilar extinction rates of the pump waves may further reduce the CFG efficiency. Therefore, at relatively low losses ($\tan\delta_{xx,zz} = 0.01$), the spectral distributions of $|F_{r,t}|$ in Figures 5a,c still qualitatively resemble those for the corresponding lossless stacks in Figure 3. Conversely, at higher losses ($\tan\delta_{xx,zz} = 0.1$), $|F_{r,t}|$ distinctively differ because the frequency mixing products emitted from the stacks are predominantly generated in a few peripheral layers adjacent to the stack outer interfaces. Therefore $|F_r|$, primarily determined by CFG at the stack front interface where the pump waves are still weakly attenuated by losses, is more than two orders of magnitude higher than $|F_t|$ of the waves emitted from the other interface. Indeed, both the pump waves, travelling through the stack, and the mixing products, generated inside the stack, are strongly attenuated due to the layer losses. Therefore the $|F_t|$ magnitude is significantly lower than $|F_r|$ as illustrated by Figures 5b,d. In this case, the stack internal composition affects the CFG efficiency primarily through linear reflection, refraction, and pump wave extinction while the role of phase coherence becomes less prominent.

Figure 5. Intensity of field radiated at frequency $\omega_3 = \omega_1 + \omega_2$ from (**a**,**b**) Fibonacci S_8 and (**c**,**d**) Thue-Morse Q_5 QPS in the reverse ($|F_r|$-solid red lines) and forward ($|F_t|$-dash-dot black lines) directions of the *z*-axis at $\omega_2 = 2.01 \times 10^{13}$ s^{-1}. The layer parameters are the same as in Figure 3a with added losses (**a**,**c**) - $\tan\delta_{xx,zz} = 0.01$ and (**b**,**d**) - $\tan\delta_{xx,zz} = 0.1$. The stack is illuminated by pump waves incident at $\Theta_{i1} = 30°$ and $\Theta_{i2} = 45°$.

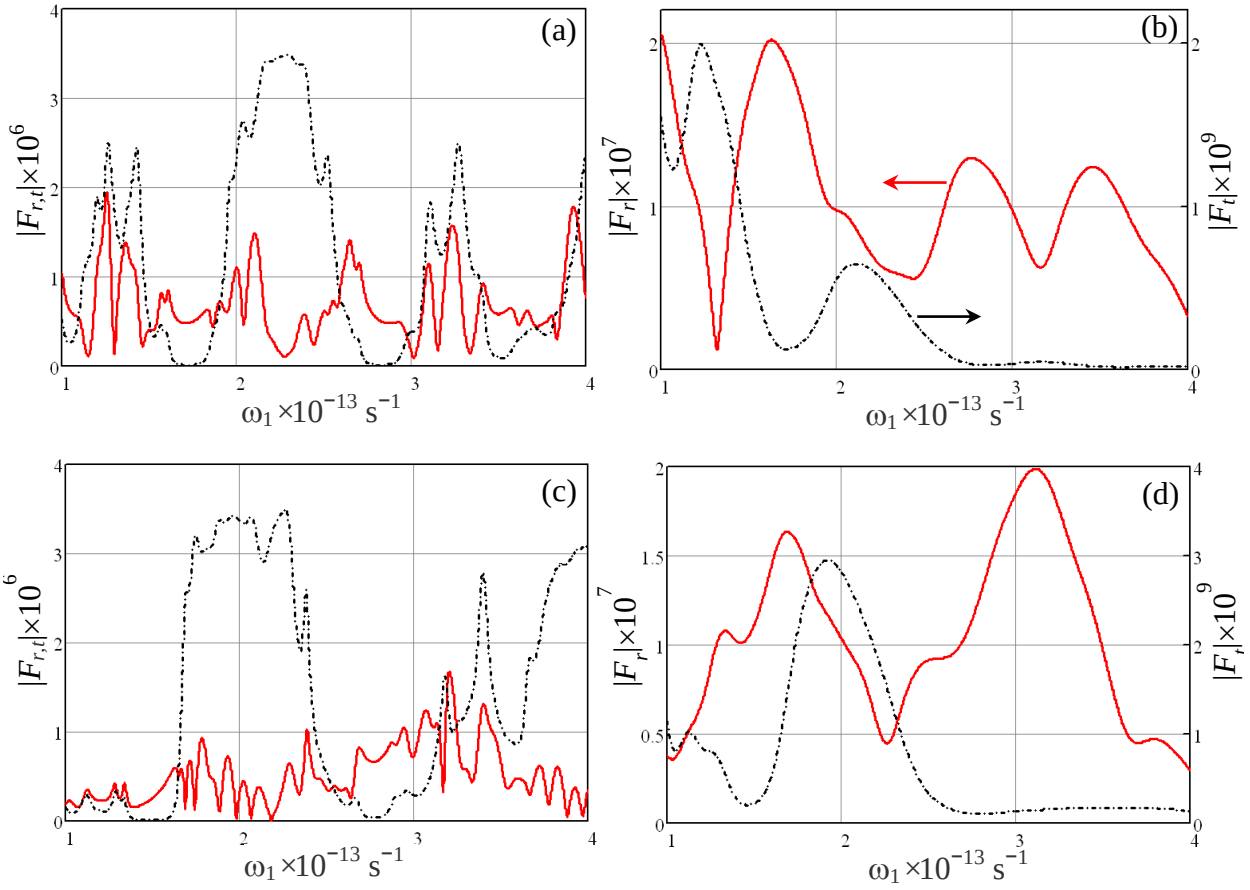

4. Conclusions

Combinatorial frequency generation (CFG) in the three-wave mixing process has been studied in the quasi-periodic stacks of binary nonlinear dielectric layers arranged in accordance with Fibonacci and Thue-Morse sequences. The closed-form solutions of the nonlinear scattering problem for QPSs, illuminated by a pair of obliquely incident pump waves of frequencies ω_1 and ω_2, have been obtained in the approximation of weak nonlinearity using the harmonic balance method. The modified TMM has been adapted to analyse QPSs similarly to perturbed periodic stacks with defects at the specified positions. It has been shown that Fibonacci and Thue-Morse QPSs can be represented as cascades of "regular" and "defective" primitive cells. The types and locations of the "defective" cells have been determined and described in analytical form. The developed theory is illustrated by the examples of numerical simulations, and the features of CFG by Fibonacci and Thue-Morse QPSs are discussed.

The simulation results have demonstrated that the nonlinear scattering coefficients $|F_{r,t}(\omega_3)|$ of combinatorial frequency $\omega_3 = \omega_1 + \omega_2$ are strongly correlated with the stack linear reflectance $|R(\omega)|$. The latter effect is attributed to the fact that $|R(\omega)|$ determines magnitudes of both the pump waves of frequencies $\omega_{1,2}$, refracted into the stacks and engaged in the frequency mixing process, and the waves

of combinatorial frequency ω_3 emitted from the stack. It has been found that the overall peak efficiency of CFG in QPSs is higher than in similar periodic stacks. The enhanced CFG in QPS is facilitated by the stack composition, which provides higher density of states, and improves the phase synchronism and local field intensification of the pump waves in the constituent layers. Comparison of CFG in Fibonacci and Thue-Morse stacks has shown that $|F_{r,t}(\omega_3)|$ peak magnitudes reach about the same levels in both types of QPSs but the peaks occur at different frequencies. At the same time, it has been observed that the layer anisotropy may affect the CFG efficiency in the low order QPSs, but its effect becomes marginal at the higher order QPSs. An extensive analysis of the CFG efficiency in lossy QPSs has shown that dissipation may qualitatively alter the frequency mixing process and change the $|F_r(\omega_3)|/|F_t(\omega_3)|$ ratio for several orders of magnitude. The latter effect is attributed to changes in the extinction scales and coherence lengths of pump waves and the CFG products.

Acknowledgments

This work has been performed in the framework of the project PEARL supported by the FP7 Marie Curie IIF Grant 255110 and short visit grant from the European Science Foundation research networking program NEWFOCUS.

Author Contributions

Oksana Shramkova and Alexander Schuchinsky jointly developed the theory, analysed results and wrote the paper. Oksana Shramkova has carried out the numerical simulations.

Appendix 1

To evaluate the fields of combinatorial frequency ω_3, it is necessary first to determine amplitudes coefficients $D_{1j,2j}^{n\pm}$ in Equation (4) for the waves generated inside each constituent layer of QPS. In the non-depleting wave approximation, this is accomplished by the harmonic balance method, which allows $D_{1j,2j}^{n\pm}(\omega_1,\omega_2)$ to be explicitly related to amplitudes $\mathcal{B}_j^{n\pm}(\omega_{1,2})$ of the pump waves of frequencies ω_1 and ω_2 refracted into each layer [40]. In contrast to regular periodic stacks, evaluation of $\mathcal{B}_j^{n\pm}(\omega)$ in QPSs is not straightforward and usually requires direct multiplication of the transfer matrices of all layers one by one. An alternative approach, based upon the QPS decomposition in "regular" and "defective" unit cells, is outlined in Section 2 and further elaborated here.

In the case of Fibonacci QPS defined in Section 2, the periodicity of the regular cells {*AB*} is perturbed by additional layers of type *A*, which form the "defective" cells {*AAB*} with layer *A* in front of the regular cells. The "regular" and "defective" cells are the primitive cells of any Fibonacci QPS S_q of order *q*. For example, in Fibonacci QPS S_5 = {*AB AAB AB A*}, the 2nd cell is defective, *i.e.*, it contains a layer *A* doublet of thickness $d'_A = 2d_A$. The regular and defective cells have the same layer sequence but different thicknesses: $d = d_A + d_B$ and $d' = d'_A + d_B$, respectively. Additionally, at odd *q* an extra layer *A* appears at the stack end, cf. S_5 above and S_6 in Section 2.

The overall number N_q of primitive cells (regular and defective) in Fibonacci QPS of order *q* is:

$$N_q = \begin{cases} \dfrac{\Phi_{q+1} - \Gamma_q}{2}, & q - \text{ even} \\ \dfrac{\Phi_{q+1} - \Gamma_q - 1}{2}, & q - \text{ odd} \end{cases} \tag{A1}$$

where $\Phi_q = \Phi_{q-1} + \Phi_{q-2}$ is Fibonacci number and $\Phi_1 = \Phi_2 = 1$; Γ_q is the number of defective cells: $\Gamma_q = 0$ at $q \le 3$, and at $q \ge 4$.

$$\Gamma_q = \begin{cases} \dfrac{\left(\dfrac{3+\sqrt{5}}{2}\right)^{\frac{q}{2}-1} - \left(\dfrac{3-\sqrt{5}}{2}\right)^{\frac{q}{2}-1}}{\sqrt{5}}, & q - \text{ even} \\ \Gamma_{q+1} - \Gamma_{q-1} - 1, & q - \text{ odd} \end{cases} \tag{A2}$$

The positions of additional *A* layers in Fibonacci QPS of order *q*, can be determined with the aid of a row-matrix $\hat{P}_q$ of length Φ_{q+1}, composed of 0's and 1's. The 1's are located only in the columns corresponding to the first *A* layer of the doublets. At $q \ge 4$, $\hat{P}_q$ is defined by the recurrence relations:

$$\hat{P}_q = \hat{P}_{q-1} + \hat{P}_{q-2}\hat{\Psi}\left(\Phi_q\right) + \begin{cases} \hat{u}\left(\Phi_q\right), & q - \text{even} \\ 0, & q - \text{odd} \end{cases} \tag{A3}$$

where $\hat{u}\left(\Phi_q\right) = \left\{\delta_{i,\Phi_q}\right\}$ is a row-matrix with 1's in the Φ_q column only, $\delta_{i,i'}$ is Kronecker delta; $\hat{\Psi}\left(\Phi_q\right) = \left\{\delta_{i+\Phi_q,j}\right\}$ is a square Toeplitz matrix with 1's only at the secondary diagonal offset for Φ_q from the main diagonal. Then the serial number $\nu_i(q)$, $i = 1,2, \ldots \Gamma_q$ of each defective cell in the stack can be deduced from $\hat{P}_q$ evaluated recursively in Equation (A3) for Fibonacci QPS of arbitrary order *q*:

$$\nu_i(q) = \frac{o_i\left(q\right) - i}{2} + 1, \tag{A4}$$

where $o_i(q)$ is the column number of the *i*th 1's in $\hat{P}_q$.

Thue-Morse QPS can be treated in a similar manner by representing a stack as a cascade of equal number of the regular {*AB*} and defective {*BA*} cells of the same thickness. The total number of primitive cells here is $N_q = 2^{q-1}$. The positions of the regular and defective cells, determined by their serial number *n* in the stack, can be deduced using the following recurrence relation at $n \ge 3$:

$$t_n = \begin{cases} 1 - t_{n-1}, & n - \text{ even} \\ t_{\left(\frac{n-1}{2}+1\right)}, & n - \text{ odd} \end{cases} \tag{A5}$$

where $t_n = 0$ represents the regular cells {*AB*} and $t_n = 1$ − defective cells {*BA*}; $t_1 = 0$, $t_2 = 1$.

Once the positions of the regular and defective cells in QPS are determined, TMM can be applied to evaluating the pump wave scattering characteristics and fields inside each layer. Magnetic field $H_y\left(\omega_p, x, z\right)$ of TM wave of frequency ω_p outside the stack has the following form:

$$H_y\left(\omega_p, x, z\right) = \mathcal{A}_p \mathrm{e}^{-i\omega_p t + ik_{xp}x} \begin{cases} \mathrm{e}^{ik_{za}^{(p)}z} + R\left(\omega_p\right)\mathrm{e}^{-ik_{za}^{(p)}z}, & z \le 0 \\ T\left(\omega_p\right)\mathrm{e}^{ik_{za}^{(p)}z}, & z \ge L_q \end{cases} \tag{A6}$$

and inside a layer of type $j = A, B$ in an nth primitive cell

$$H_{yj}^{(n)}\left(\omega_p, x, z\right) = \left(\mathcal{B}_j^{n+}\left(\omega_p\right)\mathrm{e}^{ik_{zj}^{(p)}z} + \mathcal{B}_j^{n-}\left(\omega_p\right)\mathrm{e}^{-ik_{zj}^{(p)}z}\right)\mathrm{e}^{-i\omega_p t + ik_{xp}x}, \tag{A7}$$

where $k_{xp} = k_p\sqrt{\varepsilon_a}\sin\Theta_{ip}$, $k_{za}^{(p)} = k_p\sqrt{\varepsilon_a}\cos\Theta_{ip}$ and $k_{zj}^{(p)} = \sqrt{\left(k_p^2 - \dfrac{k_{xp}^2}{\varepsilon_{zzj}}\right)\varepsilon_{xxj}}$ are the transverse and longitudinal wavenumbers outside the stack and inside the layers at frequencies ω_p, p = 1,2,3; $k_p = \omega_p/c$, c is the speed of light; A_p are amplitudes of the incident waves. $\mathcal{B}_j^{n\pm}\left(\omega_p\right)$ are amplitude coefficients of the field in individual layers.

The stack reflection $R(\omega_p)$ and transmission $T(\omega_p)$ coefficients are obtained by interrelating the fields at the stack outer interfaces with the aid of the transfer matrix $\widehat{M}_q\left(\omega_p\right)$:

$$\begin{pmatrix} H_{yA}\left(\omega_p, x, 0\right) \\ E_{xA}\left(\omega_p, x, 0\right) \end{pmatrix} = \widehat{M}_q\left(\omega_p\right)\begin{pmatrix} H_{ys}\left(\omega_p, x, L_q\right) \\ E_{xs}\left(\omega_p, x, L_q\right) \end{pmatrix} \tag{A8}$$

where subscript s in RHS identifies the type of the last layer (A or B), which depends on the QPS type and order q:

$$\text{Fibonacci sequence: } s = \begin{cases} A, & q - \text{odd} \\ B, & q - \text{even} \end{cases}$$

$$\text{Thue-Morse sequence: } s = \begin{cases} A, & q - \text{even} \\ B, & q - \text{odd} \end{cases}$$

Making use of Equations (A6) and (A8) to satisfy the continuity conditions for the tangential fields at the stack outer interfaces, we obtain the QPS reflection and transmission coefficients:

$$\begin{aligned} R\left(\omega_p\right) &= \frac{M_{q11}\left(\omega_p\right) + \dfrac{k_{za}^{(p)}}{\varepsilon_a k_p}M_{q12}\left(\omega_p\right) - \dfrac{\varepsilon_a k_p}{k_{za}^{(p)}}M_{q21}\left(\omega_p\right) - M_{q22}\left(\omega_p\right)}{M_{q11}\left(\omega_p\right) + \dfrac{k_{za}^{(p)}}{\varepsilon_a k_p}M_{q12}\left(\omega_p\right) + \dfrac{\varepsilon_a k_p}{k_{za}^{(p)}}M_{q21}\left(\omega_p\right) + M_{q22}\left(\omega_p\right)} \\ T\left(\omega_p\right) &= \frac{2}{M_{q11}\left(\omega_p\right) + \dfrac{k_{za}^{(p)}}{\varepsilon_a k_p}M_{q12}\left(\omega_p\right) + \dfrac{\varepsilon_a k_p}{k_{za}^{(p)}}M_{q21}\left(\omega_p\right) + M_{q22}\left(\omega_p\right)} \end{aligned} \tag{A9}$$

The transfer matrices $\widehat{M}_q\left(\omega_p\right)$ are evaluated by TMM at each frequency ω_p. For Fibonacci QPS, $\widehat{M}_q\left(\omega_p\right)$ is defined recursively at $q \ge 2$.

$$\widehat{M}_q\left(\omega_p\right)=\widehat{M}_{q-1}\left(\omega_p\right)\widehat{M}_{q-2}\left(\omega_p\right)$$

where $\widehat{M}_0\left(\omega_p\right)=\widehat{m}_{LB}\left(d_B,\omega_p\right)$, $\widehat{M}_1\left(\omega_p\right)=\widehat{m}_{LA}\left(d_A,\omega_p\right)$; $\widehat{m}_{LA}\left(d_A,\omega_p\right)$ and $\widehat{m}_{LB}\left(d_B,\omega_p\right)$ are the transfer matrices of layers *A* and *B*, respectively.

For Thue-Morse QPS at $q \geq 1$:

$$\widehat{M}_q\left(\omega_p\right)=\widehat{M}_{q-1}\left(\omega_p\right)\widehat{M}'_{q-1}\left(\omega_p\right)$$
$$\widehat{M}'_q\left(\omega_p\right)=\widehat{M}'_{q-1}\left(\omega_p\right)\widehat{M}_{q-1}\left(\omega_p\right)$$

with $\widehat{M}_0\left(\omega_p\right)=\widehat{m}_{LA}\left(d_A,\omega_p\right)$, $\widehat{M}'_0\left(\omega_p\right)=\widehat{m}_{LB}\left(d_{B,}\omega_p\right)$.

Once $R(\omega_p)$ and $T(\omega_p)$ are determined, amplitude coefficients $\mathcal{B}_j^{n\pm}\left(\omega_p\right)$ can be progressively deduced for each layer using the transfer matrices. In contrast to regular periodic structures, the direct evaluation of $\mathcal{B}_j^{n\pm}\left(\omega_p\right)$ for QPS is rather involved. The approach developed in this paper, where the QPSs are formed by cascading the regular and defective primitive cells, dramatically simplifies the analysis. The conventional procedure utilised for the periodic stacks can be adopted here as long as the positions of the defective cells are determined. Then the field amplitudes $\mathcal{B}_j^{n\pm}\left(\omega_p\right)$ in each layer can be expressed in the following form

$$\begin{aligned}\mathcal{B}_j^{n\pm}\left(\omega_p\right)=&\left(\eta_{j11}^{(n)}\left(\omega_p\right)\pm\frac{k_p}{k_{zLj}^{(p)}}\varepsilon_{xxj}\eta_{j21}^{(n)}\left(\omega_p\right)\right)\left(1+R\left(\omega_p\right)\right)\\&+\frac{k_{za}^{(p)}}{k_p\varepsilon_a}\left(\eta_{j12}^{(n)}\left(\omega_p\right)\pm\frac{k_p}{k_{zLj}^{(p)}}\varepsilon_{xxj}\eta_{j22}^{(n)}\left(\omega_p\right)\right)\left(1-R\left(\omega_p\right)\right)\end{aligned} \tag{A10}$$

where $\widehat{\eta}_j^{(n)}$ are the transfer matrices of a subset of $(n-1)$ primitive cells preceding the layer of type $j = A, B$ in the nth primitive cell:

$$\begin{aligned}\widehat{\eta}_A^{(n)}\left(\omega_p\right)&=\prod_{\ell=1}^{n-1}\widehat{\kappa}^{(\ell)}\left(\omega_p\right),\\ \widehat{\eta}_B^{(n)}\left(\omega_p\right)&=\widehat{\eta}_A^{(n)}\left(\omega_p\right)\widehat{\kappa}_L^{(n)}\left(\omega_p\right)\end{aligned} \tag{A11}$$

where

$$\widehat{\kappa}^{(\ell)}\left(\omega_p\right)=\begin{cases}\widehat{m}_{LA}\left(d_A,\omega_p\right)\widehat{m}_{LB}\left(d_B,\omega_p\right)-\text{regular cells in Fibonacci QPS: } \ell\neq\nu_i(q) \text{ and}\\ \qquad\qquad\text{Thue-Morse QPS: } t_\ell=0\\ \widehat{m}_{LA}\left(d'_A,\omega_p\right)\widehat{m}_{LB}\left(d_B,\omega_p\right)-\text{defective cells in Fibonacci QPS: } \ell=\nu_i(q);\ i=1,2,...,\Gamma_q\\ \widehat{m}_{LB}\left(d_B,\omega_p\right)\widehat{m}_{LA}\left(d_A,\omega_p\right)-\text{ defective cells in Thue-Morse QPS: } t_\ell=1\end{cases}$$

and

$$\widehat{\kappa}_L^{(n)}\left(\omega_p\right)=\begin{cases}\widehat{m}_{LA}\left(d_A,\omega_p\right)-\text{regular cells in Fibonacci QPS: } n\neq\nu_i(q) \text{ and}\\ \qquad\qquad\text{Thue-Morse QPS: } t_n=0\\ \widehat{m}_{LA}\left(d'_A,\omega_p\right)-\text{ defective cells in Fibonacci QPS: } n=\nu_i(q);\ i=1,2,...,\Gamma_q\\ \widehat{m}_{LB}\left(d_B,\omega_p\right)-\text{ defective cells in Thue-Morse QPS: } t_n=1\end{cases}$$

Appendix 2

The TM wave magnetic field $H_y(\omega_3)$ of frequency ω_3 emitted from the stack at combinatorial frequency ω_3 has the form:

$$H_y^a\left(\omega_3\right)=\mathrm{e}^{-i\omega_3 t+ik_{x3}x}\begin{cases}F_r\mathrm{e}^{-ik_{za}^{(3)}z}, & z\le 0\\ F_t\mathrm{e}^{ik_{za}^{(3)}z}, & z\ge L_q\end{cases}, \tag{A12}$$

where $k_{za}^{(3)}=\sqrt{k_3^2\varepsilon_a-k_{x3}^2}$ is the longitudinal wave number in the surrounding homogeneous media. To evaluate the field amplitudes $F_{r,t}$ in Equation (A12), it is necessary to relate the fields of the nonlinear products generated inside the stack to the field emitted from the QPS. This is accomplished by enforcing the tangential field continuity at the stack external interfaces and applying the modified TMM [40] to find the fields inside the stack. The fields at the stack outer interfaces of Fibonacci QPS are related as follows

$$\begin{pmatrix}H_{yA}^{(1)}\left(\omega_3,x,0\right)\\ E_{xA}^{(1)}\left(\omega_3,x,0\right)\end{pmatrix}=\hat{M}_q\left(\omega_3\right)\begin{pmatrix}H_{ys}^{(N_q)}\left(\omega_3,x,L_q\right)\\ E_{xs}^{(N_q)}\left(\omega_3,x,L_q\right)\end{pmatrix}+\sum_{n=1}^{N_q}\left[\hat{\eta}_B^{(n)}\left(\omega_3\right)\begin{pmatrix}\tau_A^{(n)}\\ \xi_A^{(n)}\end{pmatrix}+\hat{\eta}_A^{(n+1)}\left(\omega_3\right)\begin{pmatrix}\tau_B^{(n)}\\ \xi_B^{(n)}\end{pmatrix}\right]+$$
$$\begin{cases}\hat{\eta}_{N_q}\left(\omega_3\right)\hat{m}_{LA}\left(d_A,\omega_3\right)\begin{pmatrix}\tau_A^{(N_q+1)}\\ \xi_A^{(N_q+1)}\end{pmatrix}, & q\text{- odd},\\ 0, & q\text{- even},\end{cases} \tag{A13}$$

where N_q is the number of primitive cells in the stack; $\hat{\eta}_{N_q}\left(\omega_3\right)=\hat{M}_q\left(\omega_3\right)$ and $\hat{\eta}_j^{(n)}\left(\omega_3\right)$ are defined in (A1.11); $\tau_j^{(n)}$ and $\xi_j^{(n)}$ at $j = A, B$ are:

$$\begin{aligned}\tau_j^{(n)}&=D_{1j}^{n+}\sigma_{1j}^{n+}\left(k_{zj}^{+}\right)+D_{2j}^{n+}\sigma_{1j}^{n-}\left(k_{zj}^{+}\right)+D_{1j}^{n-}\sigma_{1j}^{n+}\left(k_{zj}^{-}\right)+D_{2j}^{n-}\sigma_{1j}^{n-}\left(k_{zj}^{-}\right)\\ \xi_j^{(n)}&=D_{1j}^{n+}\sigma_{2j}^{n+}\left(k_{zj}^{+}\right)+D_{2j}^{n+}\sigma_{2j}^{n-}\left(k_{zj}^{+}\right)+D_{1j}^{n-}\sigma_{2j}^{n+}\left(k_{zj}^{-}\right)+D_{2j}^{n-}\sigma_{2j}^{n-}\left(k_{zj}^{-}\right),\end{aligned} \tag{A14}$$

$D_{1j,2j}^{n\pm}$ introduced in Equation (4) are proportional to the pump wave amplitude products: $\mathcal{B}_j^{n\pm}\left(\omega_1\right)\mathcal{B}_j^{n\pm}\left(\omega_2\right)$ [40].

$$\sigma_{1j}^{n\pm}\left(\upsilon\right)=\left(\cos k_{zj}^{(3)}d_j^{(n)}-\mathrm{e}^{\pm i\upsilon d_j^{(n)}}\right)\pm i\frac{\upsilon}{k_{zj}^{(3)}}\sin k_{zj}^{(3)}d_j^{(n)};$$
$$\sigma_{2j}^{n\pm}\left(\upsilon\right)=\frac{\upsilon}{k_3\varepsilon_{xxj}}\left[i\frac{k_{zj}^{(3)}}{\upsilon}\sin k_{zj}^{(3)}d_j^{(n)}\pm\left(\cos k_{zj}^{(3)}d_j^{(n)}-\mathrm{e}^{\pm i\upsilon d_j^{(n)}}\right)\right],$$
$$d_B^{(n)}=d_B,\qquad d_A^{(n)}=\begin{cases}d_A-\text{regular cells}\\ d_A'-\text{defective cells}\end{cases}.$$

Similarly, the fields at the stack outer interfaces of Thue-Morse QPS are related as follows:

$$\begin{pmatrix}H_{yA}^{(1)}\left(\omega_3,x,0\right)\\ E_{xA}^{(1)}\left(\omega_3,x,0\right)\end{pmatrix}=\hat{M}_q\left(\omega_3\right)\begin{pmatrix}H_{ys}^{(N_q)}\left(\omega_3,x,L_q\right)\\ E_{xs}^{(N_q)}\left(\omega_3,x,L_q\right)\end{pmatrix}+\sum_{n=1}^{N_q}\left[\hat{\eta}_B^{(n)}\left(\omega_3\right)\begin{pmatrix}\tau_1^{(n)}\\ \xi_1^{(n)}\end{pmatrix}+\hat{\eta}_A^{(n+1)}\left(\omega_3\right)\begin{pmatrix}\tau_2^{(n)}\\ \xi_2^{(n)}\end{pmatrix}\right] \tag{A15}$$

where $\hat{\eta}_j^{(n)}(\omega_3)$ are defined in Equation (A11); $\tau_{1,2}^{(n)}$ and $\xi_{1,2}^{(n)}$ are as follows

$$\tau_1^{(n)} = \begin{cases} \tau_A^{(n)} - \text{regular cells} \\ \tau_B^{(n)} - \text{defective cells} \end{cases} \qquad \tau_2^{(n)} = \begin{cases} \tau_B^{(n)} - \text{regular cells} \\ \tau_A^{(n)} - \text{defective cells} \end{cases}$$

$$\xi_1^{(n)} = \begin{cases} \xi_B^{(n)} - \text{regular cells} \\ \xi_A^{(n)} - \text{defective cells} \end{cases} \qquad \xi_2^{(n)} = \begin{cases} \xi_A^{(n)} - \text{regular cells} \\ \xi_B^{(n)} - \text{defective cells} \end{cases}$$

$\tau_j^{(n)}$ and $\xi_j^{(n)}$, $j = A, B$ have the form of Equation (A14) except the layer A thickness remaining the same in both regular and defective cells, *i.e.*, $d_A^{(n)} = d_A$.

Combining Equation (A12) with Equations (A14) or (A15) in the boundary conditions for the field continuity at the stack external interfaces gives amplitudes $F_{r,t}$ of the waves emitted from the QPS at combinatorial frequency ω_3:

$$\begin{aligned} F_r &= \left(\frac{k_3 \varepsilon_a}{k_{za}^{(3)}} \hat{\eta}_{N_q}(\omega_3)_{2,1} + \hat{\eta}_{N_q}(\omega_3)_{2,2} \right) \lambda_1 - \left(\frac{k_3 \varepsilon_a}{k_{za}^{(3)}} \hat{\eta}_{N_q}(\omega_3)_{1,1} + \hat{\eta}_{N_q}(\omega_3)_{1,2} \right) \lambda_2, \\ F_t &= -\left(\lambda_1 + \lambda_2 \frac{k_3 \varepsilon_a}{k_{za}^{(3)}} \right), \end{aligned} \tag{A16}$$

where $\hat{\eta}_j^{(n)}(\omega_3)$ are defined in (A.11) and $\lambda_{1,2}$ are

- for Fibonacci QPS:

$$\lambda_r = \frac{1}{\Delta} \sum_{n=2}^{N_q} \left[\hat{\eta}_B^{(n)}(\omega_3)_{r,1} \tau_A^{(n)} + \hat{\eta}_B^{(n)}(\omega_3)_{r,2} \xi_A^{(n)} + \hat{\eta}_A^{(n+1)}(\omega_3)_{r,1} \tau_B^{(n)} + \hat{\eta}_A^{(n+1)}(\omega_3)_{r,2} \xi_B^{(n)} \right] +$$
$$+ \begin{cases} \left[\hat{\eta}_{N_q} \hat{m}_{LA}(d_A, \omega_3) \right]_{r,1} \tau_A^{(N_q+1)} + \left[\hat{\eta}_{N_q} \hat{m}_{LA}(d_A, \omega_3) \right]_{r,2} \xi_A^{(N_q+1)}, & q\text{- odd} \\ 0, & q\text{- even} \end{cases} \qquad r = 1, 2;$$

- for Thue-Morse QPS:

$$\lambda_r = \frac{1}{\Delta} \sum_{n=2}^{N_q} \left[\hat{\eta}_B^{(n)}(\omega_3)_{r,1} \tau_1^{(n)} + \hat{\eta}_B^{(n)}(\omega_3)_{r,2} \xi_1^{(n)} + \hat{\eta}_A^{(n+1)}(\omega_3)_{r,1} \tau_2^{(n)} + \hat{\eta}_A^{(n+1)}(\omega_3)_{r,2} \xi_2^{(n)} \right], \quad r = 1, 2$$

$$\Delta = \hat{\eta}_{N_q}(\omega_3)_{1,1} + \hat{\eta}_{N_q}(\omega_3)_{2,2} + \frac{k_{za}^{(3)}}{k_3 \varepsilon_a} \hat{\eta}_{N_q}(\omega_3)_{1,2} + \frac{k_3 \varepsilon_a}{k_{za}^{(3)}} \hat{\eta}_{N_q}(\omega_3)_{2,1}$$

Conflicts of Interest

The authors declare no conflict of interest.

References and Notes

1. Valy Vardeny, Z.; Nahata, A.; Agrawal, A. Optics of photonic quasicrystals. *Nat. Photon.* **2013**, *7*, 177–187.
2. Merlin, R.; Bajema, K.; Clarke, R.; Juang, F.-Y.; Bhattacharya, P.K. Quasiperiodic GaAs-AlAs Heterostructures. *Phys. Rev. Lett.* **1985**, *55*, 1768–1770.

3. Pelster, R.; Gasparian, V.; Nimtz, G. Propagation of plane waves and of waveguide modes in quasiperiodic dielectric heterostructures. *Phys. Rev. E* **1997**, *55*, 7645–7655.
4. Liu, N. Propagation of light waves in Thue-Morse dielectric multilayers. *Phys. Rev. B* **1997**, *55*, 3543–3547.
5. Maciá, E. Hierarchical description of phonon dynamics on finite Fibonacci superlattices. *Phys. Rev. B* **2006**, *73*, doi:10.1103/PhysRevB.73.184303.
6. Albuquerque, E.L.; Cottam, M.G. *Polaritons in Periodic and Quasiperiodic Structures*; Elsevier: Amsterdam, The Netherland, 2004.
7. Zoorob, M.E.; Chariton, M.D.B.; Parker, G.J.; Baumberg, J.J.; Netti, M.C. Complete photonic bandgaps in 12-fold symmetric quasicrystals. *Nature* **2000**, *404*, 740–743.
8. Cojocaru, E. Omnidirectional reflection from finite periodic and Fibonacci quasi-periodic multilayers of alternating isotropic and birefringent thin films. *Appl. Opt.* **2002**, *41*, 747–755.
9. Barriuso, A.; Monzón, J.; Sánchez-Soto, L.; Felipe, A. Comparing omnidirectional reflection from periodic and quasiperiodic one-dimensional photonic crystals. *Opt. Exp.* **2005**, *13*, 3913–3920.
10. Freedman, B.; Bartal, G.; Segev, M.; Lifshitz, R.; Christoet, D.N. Wave and defect dynamics in nonlinear photonic quasicrystals. *Nature* **2006**, *440*, 1166–1169.
11. El Hassouani, Y.; Aynaou, H.; El Boudouti, E.H.; Djafari-Rouhani, B.; Akjouj, A.; Velasco, V.R. Surface electromagnetic waves in Fibonacci superlattices: Theoretical and experimental results. *Phys. Rev. B* **2006**, *74*, doi:10.1103/PhysRevB.74.035314.
12. Moretti, L.; Rea, I.; Rotiroti, L.; Rendina, I.; Abbate, G.; Marino, A.; de Stefano, L. Photonic band gaps analysis of Thue-Morse multilayers made of porous silicon. *Opt. Exp.* **2006**, *14*, 6264–6272.
13. Makarava, L.N.; Nazarov, M.M.; Ozheredov, I.A.; Shkurinov, A.P.; Smirnov, A.G.; Zhukovsky, S.V. Fibonacci-like photonic structure for femtosecond pulse compression. *Phys. Rev. E* **2007**, *75*, doi:10.1103/PhysRevE.75.036609.
14. Tuz, V. Optical properties of a quasi-periodic generalized Fibonacci structure of chiral and material layers. *JOSA B* **2009**, *26*, 627–632.
15. Reyes-Gómez, E.; Raigoza, N.; Cavalcanti, S.B.; de Carvalho, C.A.A.; Oliveira, L.E. Plasmon polaritons in photonic metamaterial Fibonacci superlattices. *Phys. Rev. B* **2010**, *81*, doi:10.1103/PhysRevB.81.153101.
16. Pang, X.-N.; Dong, J.-W.; Wang, H.-Z. Photonic localization of interface modes at the boundary between metal and Fibonacci quasiperiodic structure. *JOSA B* **2010**, *27*, 2009–2013.
17. Olkhovskiy, Y.A.; Shramkova, O.V. Electromagnetic wave transmission and reflection by a quasiperiodic layered semiconductor structure. *Phys. B Condens. Matter* **2011**, *406*, 1415–1419.
18. Dolev, I.; Volodarsky, M.; Porat, G.; Arie, A. Multiple coupling of surface plasmons in quasiperiodic gratings. *Opt. Lett.* **2011**, *36*, 1584–1586.
19. Hsueh, W.J.; Wun, S.J.; Lin, Z.J.; Cheng, Y.H. Features of the perfect transmission in Thue-Morse dielectric multilayers. *J. Opt. Soc. Am. B* **2011**, *28*, 2584–2591.
20. Hsueh, W.J.; Chang, C.H.; Cheng, Y.H.; Wun, S.J. Effective Bragg conditions in a one-dimensional quasicrystal. *Opt. Expr.* **2012**, *20*, 26618–26623.
21. Kruk, S.S.; Helgert, C.; Decker, M.; Staude, I.; Menzel, C.; Etrich, C.; Rockstuhl, C.; Jagadish, C.; Pertsch, T.; Neshev, D.N.; *et al*. Optical metamaterials with quasicrystalline symmetry: Symmetry-induced optical isotropy. *Phys. Rev. B* **2013**, *88*, doi:10.1103/PhysRevB.88.201404.

22. Savoia, S.; Castaldi, G.; Galdi, V. Optical nonlocality in multilayered hyperbolic metamaterials based on Thue-Morse superlattices. *Phys. Rev. B* **2013**, *87*, doi:10.1103/PhysRevB.87.235116.
23. Xu, S.; Zhu, Y.; Wang, L.; Yang, P.; Chu, P.K. Passband and defective bands in photonic and quasi-crystals. *J. Opt. Soc. Am. B* **2014**, *31*, 664–671.
24. Gong, Y.; Liu, X.; Wang, L.; Lu, H.; Wang, G. Multiple responses of TPP-assisted near-perfect absorption in metal/Fibonacci quasiperiodic photonic crystal. *Opt. Expr.* **2011**, *19*, 9759–9769.
25. Feng, J.; Zhu, Y.; Ming, N. Harmonic generations in an optical Fibonacci superlattice. *Phys. Rev. B* **1990**, *41*, 5578–5582.
26. Zhu, S.; Zhu, Y.; Ming, N. Quasi-phase-matched third-harmonic generation in a quasi-periodic optical superlattice. *Science* **1997**, *278*, 843–846.
27. Fradkin-Kashi, K.; Arie, A. Multiple-wavelength quasi-phase-matched nonlinear interactions. *IEEE J. Quant. Electron.* **1999**, *35*, 1649–1656.
28. Chern, G.-W.; Chang, J.-F.; Wang, L.A. Modeling of nonlinear pulse propagation in periodic and quasi-periodic binary long-period fiber gratings. *JOSA B* **2002**, *19*, 1497–1508.
29. Huang, T.; Huang, D. Interplay between optical nonlinearity and localization in a finite disordered Fibonacci chain. *Phys. Rev. B* **2007**, *76*, doi:10.1103/PhysRevB.76.024201.
30. Lifshitz, R.; Arie, A.; Bahabad, A. Photonic quasicrystals for nonlinear optical frequency conversion. *Phys. Rev. Lett.* **2005**, *95*, doi:10.1103/PhysRevLett.95.133901.
31. Werchner, M.; Schafer, M.; Kira, M.; Koch, S.W.; Sweet, J.; Olitzky, J.D.; Hendrickson, J.; Richards, B.C.; Khitrova, G.; Gibbs, H.M.; *et al*. One dimensional resonant Fibonacci quasicrystals: Noncanonical linear and canonical nonlinear effects. *Opt. Expr.* **2009**, *17*, 6813–6828.
32. Vasconcelos, M.S.; Mauriz, P.W.; Albuquerque, E.L. Optical filters based in quasiperiodic photonic crystal. *Microelectron. J.* **2009**, *40*, 851–853.
33. Grigoriev, V.; Biancalana, F. Bistability, multistability and non-reciprocal light propagation in Thue-Morse multilayered structures. *New J. Phys.* **2010**, *12*, doi:10.1088/1367-2630/12/5/053041.
34. Zhukovsky, S.V.; Smirnov, A.G. All-optical diode action in asymmetric nonlinear photonic multilayers with perfect transmission resonances. *Phys. Rev. A* **2011**, *83*, doi:10.1103/PhysRevA.83.023818.
35. Lotfi, E.; Jamshidi-Ghaleh, K.; Moslemi, F.; Masalehdan, H. Optical multistability in 1D photonic crystals with nonlinear Thue-Morse structure. *Appl. Phys. A* **2011**, *103*, 669–672.
36. Zhu, S.N.; Zhu, Y.Y.; Qin, Y.Q.; Wang, H.F.; Ge, C.Z.; Ming, N.B. Experimental realization of second harmonic generation in a Fibonacci optical superlattice of $LiTaO_3$. *Phys. Rev. Lett.* **1997**, *78*, 2752–2755.
37. Chen, Y.B.; Zhang, C.; Zhu, Y.Y.; Zhu, S.N.; Wang, H.T.; Ming, N.B. Optical harmonic generation in a quasi-phase-matched three-component Fibonacci superlattice $LiTaO_3$. *Appl. Phys. Lett.* **2001**, *78*, 577–579.
38. Sheng, Y.; Koynov, K.; Zhang, D. Collinear second harmonic generation of 20 wavelengths in a single two-dimensional decagonal nonlinear photonic quasi-crystal. *Opt. Commun.* **2009**, *282*, 3602–3606.
39. Blombergen, N. *Nonlinear Optics: A Lecture Note*; Benjamin: New York, NY, USA & Amsterdam, The Netherland, 1965.

40. Shramkova, O.V.; Schuchinsky, A.G. Nonlinear scattering by anisotropic dielectric periodic structures. *Adv*. *OptoElectron*. **2012**, doi:10.1155/2012/154847.
41. Jeong, Y.; Lee, B. Matrix analysis for layered quasi-phase-matched media considering multiple reflection and pump wave depletion. *IEEE J*. *Quant*. *Electron*. **1999**, *35*, 162–172.
42. Li, J.-J.; Li, Z.-Y.; Zhang, D.-Z. Second harmonic generation in one-dimensional nonlinear photonic crystals solved by the transfer matrix method. *Phys*. *Rev*. *E* **2007**, *75*, doi:10.1103/PhysRevE.75.056606.
43. Szczepański, P.; Osuch, T.; Jaroszewicz, Z. Modeling of amplification and light generation in one-dimensional photonic crystal using a multiwavelength transfer matrix approach. *Appl*. *Opt*. **2010**, *48*, 5401–5406.
44. Li, J.-J.; Li, Z.-Y.; Zhang, D.-Z. Nonlinear frequency conversion in two-dimensional nonlinear photonic crystals solved by a plane-wave-based transfer-matrix method. *Phys*. *Rev*. *B* **2008**, *77*, doi:10.1103/PhysRevB.77.195127.
45. Yariv, A.; Yeh, P. *Optical Waves in Crystals: Propagation and Control of Laser Radiation*; Wiley: New York, NY, USA, 1984.
46. The approximation of the non-depleting nonlinear process is used here. Therefore extinction of pump waves is caused by the dissipative losses only.